buildings

MDPI

Article

Research on Shield Tunneling across a River Using a Scale Model

Wenxiao Li [1], Yilei Zhang [1], Jianxun Ma [1,*] and Mohammed El Hoseny [1,2]

[1] School of Human Settlements and Civil Engineering, Xi'an Jiaotong University, Xi'an 710048, China; wenxiao-li@stu.xjtu.edu.cn (W.L.); zyl666wish@163.com (Y.Z.); mohammed.elhoseny@stu.xjtu.edu.cn (M.E.H.)

[2] Faculty of Engineering at Shoubra, Benha University, Cairo 11629, Egypt

* Correspondence: majx@xjtu.edu.cn; Tel.: +86-15102982529

Abstract: This paper proposes a scale model test to simulate shield tunnel excavation over long distances. The test simulates the whole process of shield tunneling through the Weihe River on Xi'an Metro Line 1, where the tunneling length and diameter reach 100 m and 6 m, respectively. The dimensions of the test setup were 6.0 m × 1.0 m × 1.0 m, the diameter of the tunnel model was 160 mm, and the geometric similarity ratio was 1:40. Finite element analysis and field measurements were performed to complement the test results. By comparing the finite element simulation and field measurement, the scale model test was validated and verified to be reliable. The results show that the test effectively predicts riverbed deformation caused by shield construction. In addition, it can be applied to soil stability analysis and the impact evaluation of surface deformation in other shield-crossing rivers, complex strata, and superstructure groups, providing auxiliary guidance for shield constructions.

Keywords: scale model test; shield tunneling; river; finite element analysis; long distances

Citation: Li, W.; Zhang, Y.; Ma, J.; El Hoseny, M. Research on Shield Tunneling across a River Using a Scale Model. *Buildings* **2024**, *14*, 34. https://doi.org/10.3390/buildings14010034

Academic Editor: Stefania Sica

Received: 12 October 2023
Revised: 25 November 2023
Accepted: 28 November 2023
Published: 22 December 2023

1. Introduction

A shield tunnel is the most common method in the construction of urban subways, which has the advantages of high boring speed, high efficiency, and a short construction period. When a shield tunnel is exposed to uncertainty in the soil and complex geology, such as a river and geological faults, monitoring of the tunnel and surrounding soil is required to ensure project safety [1]. In the shield construction of underground tunnels, a single theoretical calculation or numerical simulation is not enough to guide the design of the project due to project size, incomplete prediction of soil characteristics, and complex construction conditions. However, model tests can reproduce engineering phenomena in the laboratory with scale models, which helps to solve this problem.

Model tests help the observation of test phenomena at a macroscopic level and the measurement of data that are difficult to obtain in real projects, playing a very important role in shield construction [2]. Model tests for shields can be divided into three categories: the "ng" test, represented by the centrifugal test, which scales by 1/n and increases gravitational acceleration by a factor of n using a centrifuge. Da Long J et al. [3] used the "ng" test to study the collapse patterns in a tunnel face and surrounding soil pressures. The test used a TK-C500 type geotechnical centrifuge, reaching a centrifugal acceleration of 150 g. The second category is the "1 g" test, satisfying physical similarity and mechanical parameters of soil with a suitable similarity ratio. Han M.S et al. [4] proposed a shield model test for soft soil foundations with a similarity ratio of 1:48, scaling the soil layer and shield machine according to this ratio. In order to satisfy the similarity criterion for soil properties, a suitable mix ratio was developed. The third category is the model tests that do not need to satisfy the similarity criterion with high accuracy, which applied to study general laws induced by shield tunneling. When studying the influence of unloading and excavation of soft clay soils on shield tunnels, Peng fei Xiang et al. [5] applied a model test with a

similarity ratio of 1:15.5, using soft clay soil sampled from a construction site. This test belongs to the third category of modeling tests because the physical properties of the soil did not meet the similarity criterion. In "ng" tests, the size of the centrifuge and scaled model is small, making the setup and operation of tests more complicated to execute. The "1 g" test satisfies the similarity ratio, yielding more accurate test results to deduce the actual state. However, it is difficult to find materials that satisfy the similarity ratio with high precision. The third type of model test does not strictly satisfy the similarity criterion, resulting in inaccurate test results. However, it is very effective for qualitatively studying complex changes in structures. The choice of the test method depends on the objectives of the study, available resources, and test conditions. Consequently, "1 g" and "ng" tests may be good for achieving high-accuracy results and similarity ratios. However, the third type of model test may be a more cost-effective option when the complexity of the test is high and only qualitative results are required.

Shield machines perform multiple functions, such as cutting, movement, segment assembly, and grouting. It is difficult to realize all these functions on a shield machine model that is scaled down n times [6]. Therefore, model tests of the shield may ignore different factors depending on the object of study. According to Saint Venant's principle, the influence of grouting at the rear of the shield and the excavation at the front is limited, especially when these two factors interact with each other. Therefore, when facial support is studied, tunnel assembly and the grouting process are ignored [7]. Kuepferle et al. [8] neglected shield tunnel segment installation and the grouting process when studying the wearing of a shield cutter head. When grouting is studied, palm face excavation is often ignored. Liu et al. [9] constructed an oversized test model with a geometric similarity ratio of 1:3 when studying tail grouting and considered grouting while ignoring palm face excavation and segment assembly.

Some scholars have also constructed fully functional shield machine models. Li et al. [10] constructed a model of an earth pressure balance shield with a diameter of 400 mm. The final test excavation distance was 1.78 m, and the C/D (excavation length/tunnel diameter) was 4.5. Hu et al. [11] constructed a shield model with a diameter of 800 mm, which can simulate the full function of a shield machine. However, due to the size effect, the shield machine model disturbs the soil too much for long excavations. Joo et al. [12] built a full-scale shield model with a diameter of 3.6 m, which was the same as the real shield machine, enabling the study of detailed parameters in shield tunneling but requiring a large test site.

The above-mentioned shield models are complex structures with high test costs, making it challenging to build them in the limited space of a laboratory. Therefore, some scholars have utilized indirect methods to simulate the shielding process in the laboratory. For example, Ding et al. [13–15] proposed an indirect modeling test for a shield using the buried pipe method, in which a shield tunnel model is pre-buried inside the soil, and the shield tunnel forming is simulated by pushing, pulling, rotating, and other operations on the pipe. In addition, they applied a double-layer tube model to simulate shield tunnel formation by gradually pulling out the outer layer of tubes. This method simplifies model tests and simulates shield tunnel formation without cutting the soil. The disadvantages are that the model cannot simulate grouting and boring, and the soil in front of the tunnel differs from reality.

Lu et al. [16] used another tunnel model test in their study of the stability of the palm face: the discrete method. This method simulates the formation of shield tunnels by repeatedly burying the tunnel model. Specifically, the soil and tunnel are re-excavated for each loop of the shield tunnel being formed. This method drives each step of the tunnel to form independently. However, there is little correlation between the different steps, resulting in the discontinuity of the tunnel-forming process.

In the background, the radius of the shield machine model and excavation distance C/D (excavation length/tunnel diameter) are shown in Figure 1. It shows that the radius of the shield machine model increases exponentially with the increase in excavation distance.

This is because the long-distance model test requires a more fully functional shield machine model and enough space to accommodate the equipment.

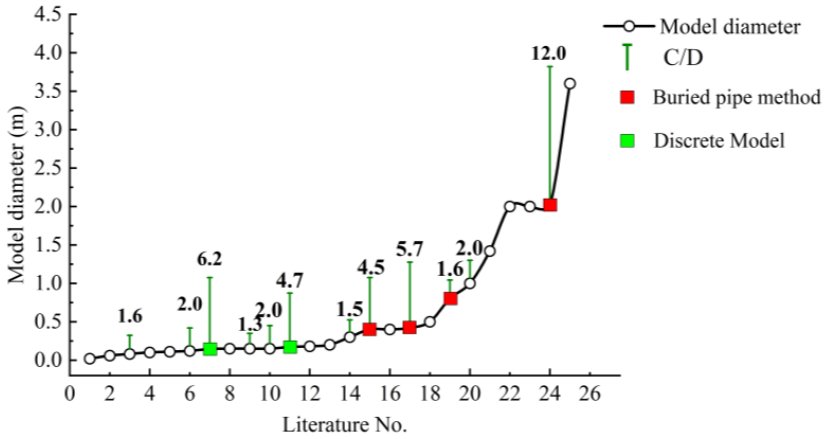

Figure 1. Shield model size curve available in the literature.

When the shield traverses complex strata, it is necessary to assess the risks encountered in the project in advance and formulate a response plan [17,18]. Traditional assessment methods mainly depend on engineers' experience and computer simulation, which cannot ensure reliability [19]. In addition, the traditional scaling test method has limited digging distance, considering the challenge of providing practical and long-term guidance for the whole process of shield construction. Therefore, a scaling test of the whole process of shield construction can be carried out in a laboratory with a limited space.

Moreover, Figure 1 shows the excavation distances of tests using the "buried pipe method" and the "discrete method", which are considered higher than those of the other tests. These two methods use equivalent test methods, avoiding soil excavation in tests and simplifying the shield machine model. However, the "buried pipe method" only reflects the state of the completed tunnel and cannot reflect stress and displacement changes during tunnel construction. The "discrete method" requires repeatedly burying tube pieces, thus complicating test steps. Therefore, this paper proposes a test method to simulate the whole shield tunneling process based on a combination of the "buried pipe method" and the "discrete method".

The test model proposed in this paper involves cutting the tunnel model and pre-embedding it in soil and then simulating the impact of a shield tunnel on the surrounding soil by applying vertical loads to the tunnel model. Compared with the "buried pipe method" and the "discrete method", this model test can simulate shield tunneling, tunnel deformation, and the soil in front of the tunnel. In particular, for long-distance shield scaling simulation, this test method has great potential. Therefore, the novelty of this paper is performing a scaled-down model test capable of long-distance shield simulation. A special unidirectional connection of the tunnel model is set up to reduce the impact of the pre-buried tunnel on the unexcavated soil in front.

2. Shield Scale Model Test

2.1. Test Background

The case study is based on Xi'an Metro Line 1, located in the middle of the Weihe Fault Basin near the fracture zone on the north bank of the Weihe River (Figure 2). There are uncertainties in the project, such as river water, fracture zone, and loess, so the whole shield model test process needs to ensure the project's safety. The project uses an SPB (Slurry Pressure Balance Shield); the basic information is shown in Table 1.

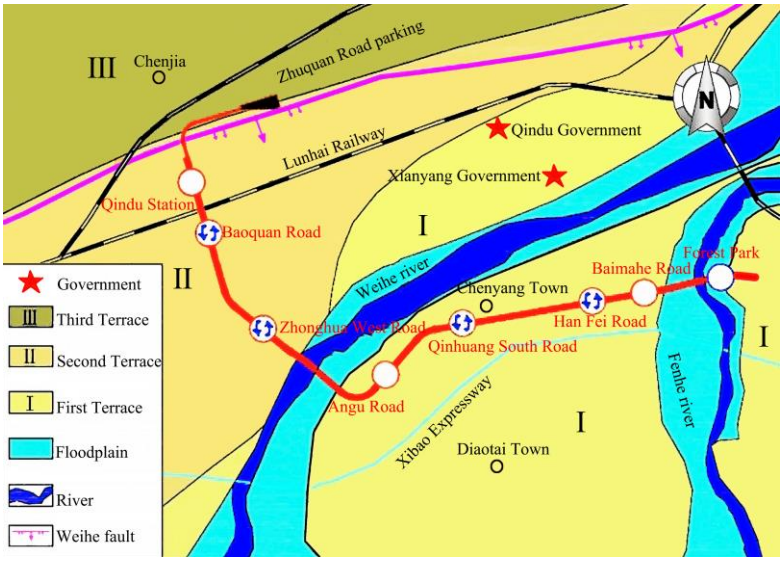

Figure 2. Project map.

Table 1. The basic information of the SPB.

Basic Information	
Tunnel length	2050 m
Excavation diameter	6.28 m
Diameter of segment	6 m
Segment length	1.5 m
Shield length	9.24 m
Auxiliary equipment length	50 m
Excavation thrust	600 t
Cutter torque	5256 kN·m
Driving speed	8 cm/min
Shield machine weight	4000 kN
Supporting system weight	1500 kN

2.2. The Test Device

The test device consists of four parts: test chamber, tunnel model, loading system, and measurement system (Figure 3). The geometric similarity ratio of the test is 1:40, and the full size of the test chamber is 6.0 m × 1.0 m × 1.0 m (length × width × depth), which is composed of tempered glass with a 12 mm thickness and steel frame (Figure 3a).

The loading system comprises loading rods, hanger rods, and a steel frame. The loading and hanger rods corresponded to the tunnel model individually, in which the hanger rods were connected to the tunnel model at one end while the other was connected to the loading rod. A sleeve separated the hanger rods from the soil, ensuring load transfer to the tunnel model. One end of the loading rod was connected to a frame, while the other was loaded with a heavy load. In the middle, it was connected to the loading rod to apply vertical load with the lever principle (Figure 3b).

The tunnel model comprised 25 special pipes, each with a 160 mm diameter and a 100 mm length. Each pipe represented three segments in the actual project (Figure 3c). Furthermore, each pipe was equipped with an upper support at the front end and a lower support at the rear end. The pipes were nested together using these supports. When pipe B moved downward, it received support from pipe A, positioned at the rear, whereas pipe C, at the front, did not provide support for pipe B. Thus, pipe A represented the completed tunnel, pipe C represented soil before the shield machine, and pipe B represented the shield machine.

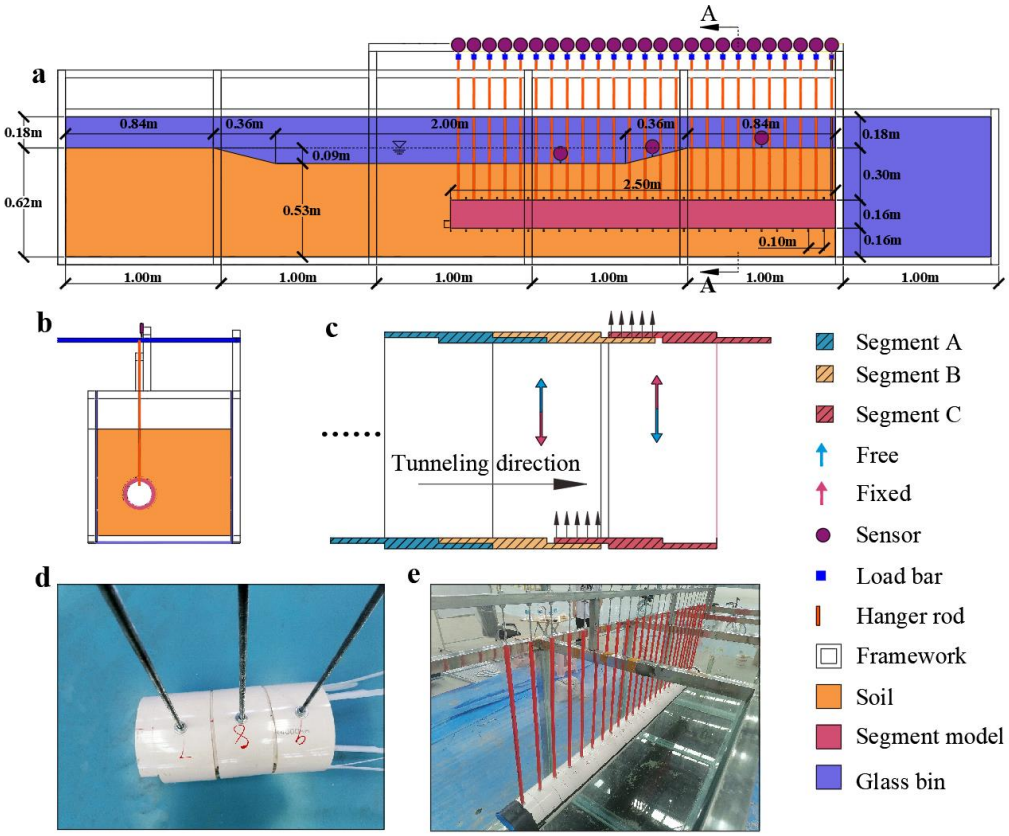

Figure 3. The test device: (**a**) front view of the test device; (**b**) A-A section view of the test device; (**c**) schematic diagram of the segment connection; (**d**) photographs of the three-section tunnel model; and (**e**) a photograph of the test chamber.

The measurement system consisted of displacement measurements of the tunnel model and settlement measurements of the soil surface (Figure 3a). Each hanger rod was equipped with a percentage meter to accurately measure the tunnel model's displacement. Three settlement measurement points were established on the soil surface, representing the riverbank, river floodplain, and deep-water area.

Figure 4 shows the distribution of soil layers in the actual project. From top to bottom, the strata within the tunnel area are coarse sand, silty clay, and medium coarse sand. The tunnel is located in the medium-coarse sand and silty clay layers. The actual soil layers are simplified in the model test, representing only the soil layer with large distribution areas. The mechanical properties of each soil layer are shown in Table 2.

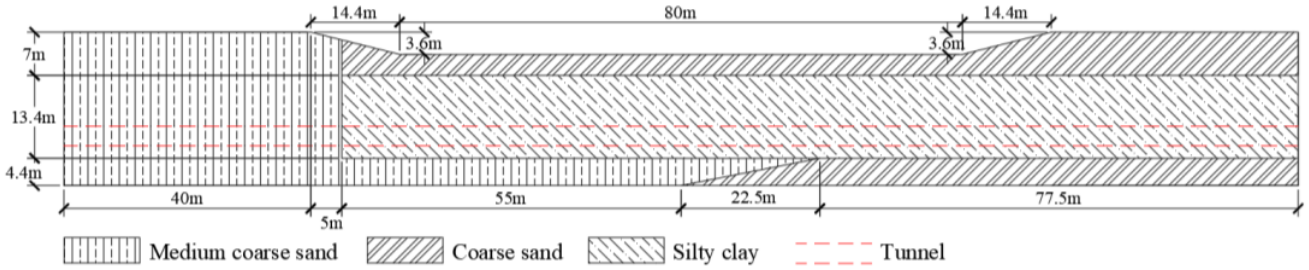

Figure 4. Soil distribution map.

Table 2. The mechanical properties of each soil layer.

Soil Layer	Coarse Sand	Silty Clay	Medium Coarse Sand
Poisson's ratio	0.35	0.3	0.25
Density (g/cm^3)	2.2	2	2
Elasticity modulus (MPa)	30	7	30
Cohesive strength (kPa)	0	30.8	5.6
Friction angle (°)	34.5	18.2	32.87
Dry density (g/cm^3)	1.77	1.64	1.74

2.3. Test Principle

The test method proposed in this paper combines the "buried tube method" and the "discrete method". The test principle is to pre-bury the separate tunnel model in soil, apply vertical loads to the tunnel model, and simulate the formation of a shield tunnel using changes in the load at different construction steps. In particular, when the dynamic disturbance of soil caused by shield excavation is not considered, forming the shield tunnel is equivalent to loading and unloading on the surrounding soil. The unloading effects result from soil excavation; soil pressure from the shield machine, tunnel, and ancillary equipment; circumferential pressure by grouting on surrounding soil; and boring pressure on the soil. Therefore, by applying different types and magnitudes of loads to pre-buried tunnels at different locations, the shield effects on surrounding soil can be simulated indirectly. Due to the small diameter of the tunnel model used in the tests, which was only 160 mm, applying the circumferential grouting pressure was difficult. In addition, the grouting pressure effects were not considered.

The pre-burial processes of the pipe were as follows: firstly, the pipe was fixed to the external frame using a hanging rod. Secondly, the soil was buried in the test tank according to the soil distribution. Thirdly, the hanger rod holding the tube was loosened. Finally, pressure was applied to the tube to restore the soil stress to the original soil stress. The soil stress distribution due to pipe burial was simulated using finite elements. In theory, when a soil layer is subjected to self-weight, and there are no pipes or other objects within the soil layer, the stress distribution within the soil is uniform at the same depth with horizontal lines on a stress diagram. However, when the soil layer is pre-buried with a pipe, the stress distribution in the soil layer after soil stabilization is not uniform, and the stress contour is not a straight line (Figure 5). After applying the vertical load (F_0), as in Equation (1), the soil layer stress contour is close to a straight line (uniform stress distribution).

$$F_0 = \beta \frac{\pi D^2}{4} \rho g H \quad (1)$$

where D is the diameter of the pipe, D = 160 mm; ρ is the average saturated density of the soil layer: ρ = 2000 kg/m^3; g is the acceleration of gravity, g = 9.8 m/s; H is the width of the pipe, H = 100 mm; and β is the stress distribution coefficient, β = 1.8.

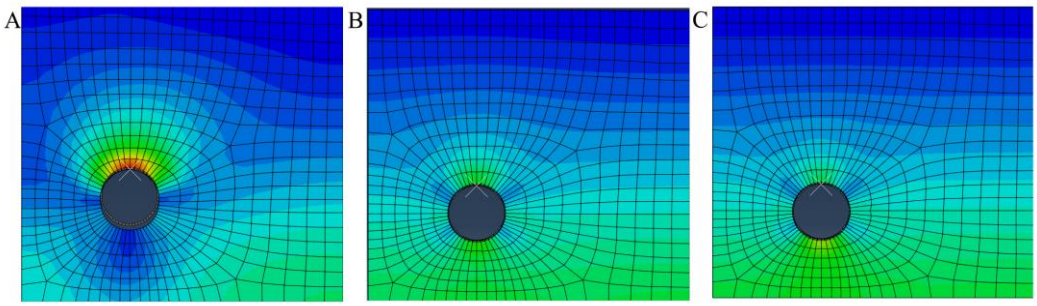

Figure 5. Soil stress distribution: (**A**) the pipe was fixed; (**B**) the hanger rod holding the pipe was loosened; and (**C**) pressure was applied to the tube.

Shield construction is divided into four stages: unexcavated, construction, transition, and completion (Figure 6). During the unexcavated stage, the tunnel model was pre-buried in the soil. After applying a vertical load of F_0, the soil stress was restored. In the construction stage, the soil was excavated and subjected to the shield machine self-weight, and the vertical load (F_T) was equal to the self-weight of the shield machine, as in Equation (2). According to Table 1, the shield machine length is 9.24 m, which is equal to two excavation units (one "excavation unit" is the length of one section of the tunnel model).

$$F_T = \frac{\alpha W_T}{2} \tag{2}$$

where W_T is the self-weight of the shield machine and α is the load similarity ratio, which is determined according to Equation (3):

$$\alpha = \frac{W_{Test}}{W_{Eng}} = \frac{V_{Test}\rho_s g}{V_{Eng}\rho_s g} = \frac{V_{Test}}{V_{Eng}} = \frac{1}{64{,}000} \tag{3}$$

where W_{Test} is the weight of soil in the test tank, W_{Eng} is the weight of soil in real condition, V_{Test} is the volume of soil in the test tank, V_{Eng} is the volume of real soil, ρ_s is the average density of the soil, and g is the acceleration of gravity, 9.8 m/s.

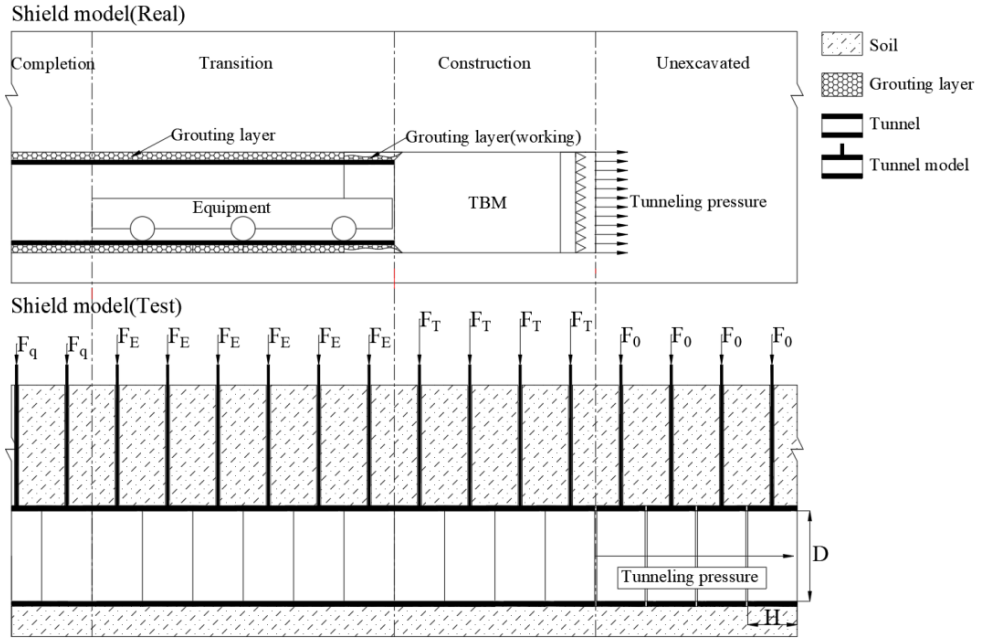

Figure 6. Schematic diagram of test loading.

In the transition stage, the soil excavation and assembly of the segments were completed. In this stage, there were tunnel and shield appurtenances in the soil, so the load F_E included the self-weight of the tunnel and the appurtenances. During the test, the appurtenant equipment length was about six times the length of a section tunnel model, and the load F_E was determined according to Equation (4).

$$F_E = \alpha \frac{W_E + W_q}{6} \tag{4}$$

where W_q is the weight of the six tunnel segments and W_E is the shield appurtenance self-weight.

In the completion stage, the shield tunnel was complete, and there were only segments in the soil, so the load Fq was determined according to Equation (5).

$$F_q = \alpha \frac{W_q}{6} \quad (5)$$

In summary, the load values of the test were determined, as shown in Table 3.

Table 3. The load values for the test.

Load	Project (kN)	Test (N)
F_0	2490	38.94
F_T	4000	62.5
F_E	1500	23.4
F_q	591	9.21

2.4. The Test Steps

The test steps were as follows:

Step 1: Installation of the tunnel model in the test tank using hanger rods.

Step 2: According to the soil layer distribution, the test tank was filled with soil layer by layer. Every 100 mm of filling was flattened with a heavy object. After filling the soil, water was injected to fill the channel. A displacement meter was placed on the soil surface, and the meter values were recorded. The soil was stabilized when the displacement of the soil surface tended to be constant. The tunnel model was not waterproof, and the soil was considered saturated when a large amount of water flowed out of the tunnel entrance.

Step 3: The test tank was filled with water until the required level.

Step 4: The fixing bolts of each hanger rod were loosened and the load of F_0 was applied.

Step 5: The displacement of the soil surface was recorded every 1 min. When the displacement tended to be constant, the soil deformation was stable. After that, the loads in Table 2 were applied.

Step 6: The tunnel model displacements were recorded every 1 min, and when the displacement tended to be constant, the soil deformation was stable. After stabilizing the soil deformation, the soil and segment displacement information were recorded.

Step 7: Step 5 and step 6 were repeated until the desired digging length was reached.

3. Test Results

The final simulated length of the test was 25 "excavation units" (one "excavation unit" is the length of one section of the tunnel model), which is equivalent to the actual project excavation length of 100 m. Among them, 12 "excavation units" were used to study the impact of shield tunneling on soil and tunnels, and 13 "excavation units" were used to study the effect of water level changes on the shield. Only the first 12 "excavation units" are studied in this paper. As shown in Figure 7, the 12 bars represent the tunnel model displacements at different boring positions. In each stage, the shield advances one "excavation unit". The purple rectangle is the shield model, which has a length of two "excavation units". The tunnel model in front of the shield is soil, and the tunnel model behind the shield (green rectangle) is the completed tunnel.

When the shield enters the soil (step 1 and step 2), the boundary effect causes the soil in front of the shield to settle, and the influence range of settlement is about 5–6 "excavation units". As the shield machine progresses (step 3 and step 4), the influence range of the shield on the soil gradually increases. Starting at step 4, the ground settlement caused by the boundary effect starts to slow down due to the shield deepening. In addition, the tunnel behind the shield machine shows a significant uplift (step 4 to step 12) due to the soil unloading reaction resulting from the shield's passage. In actual projects, the turning moment formed by the tunnel load and the shield machine's self-weight can cause the shield machine to deviate from the prescribed travel route, requiring real-time monitoring of the forward direction of the shield machine and adjusting.

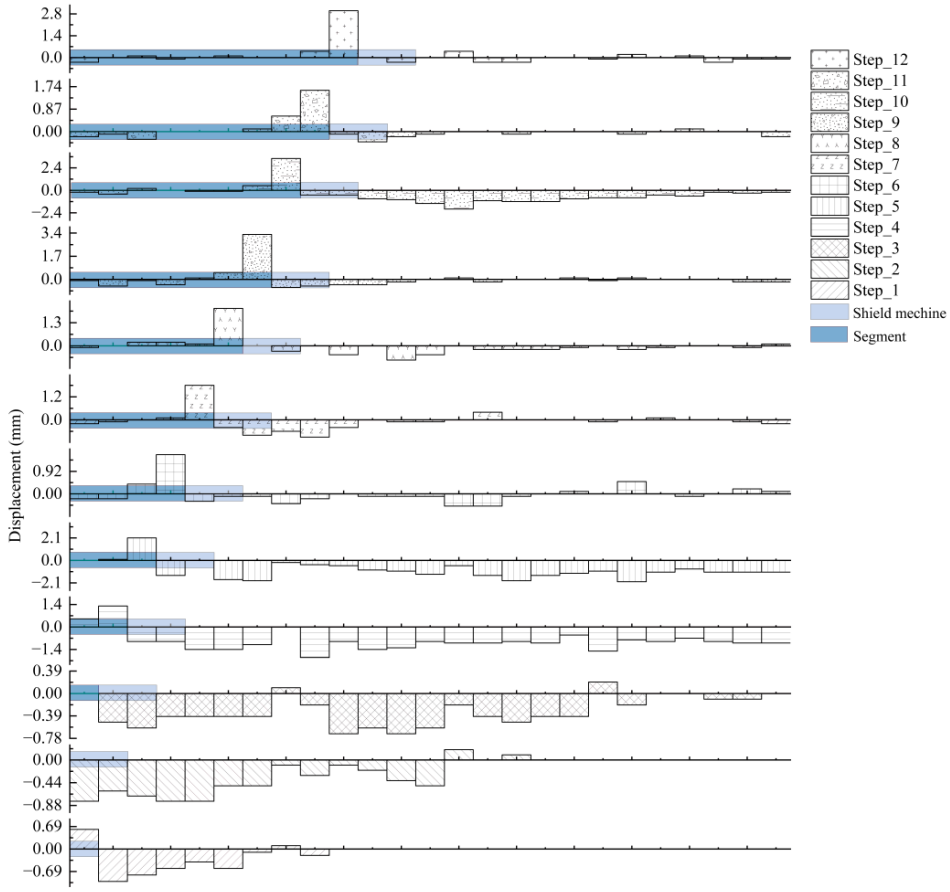

Figure 7. Displacement of the shield tunnel model.

The results of the ground displacement meter show that the shield causes substantial settlement of the ground surface above the shield machine (Figure 8). In this case, the surface settlement rate of the riverbed is greater than that of the riverbank, which differs by a factor of 3. However, the final settlement of the riverbed and riverbank is close, with a maximum settlement of 0.0780 mm on the riverbank and 0.0648 mm on the riverbed. With a similar ratio of 40:1, the maximum settlement on the riverbank becomes 3.120 mm, and the maximum settlement on the riverbed is 2.592 mm. Since the test is not a strict proportional test, the ground settlement results can only be used for qualitative analysis, and the quantitative analysis is for reference only.

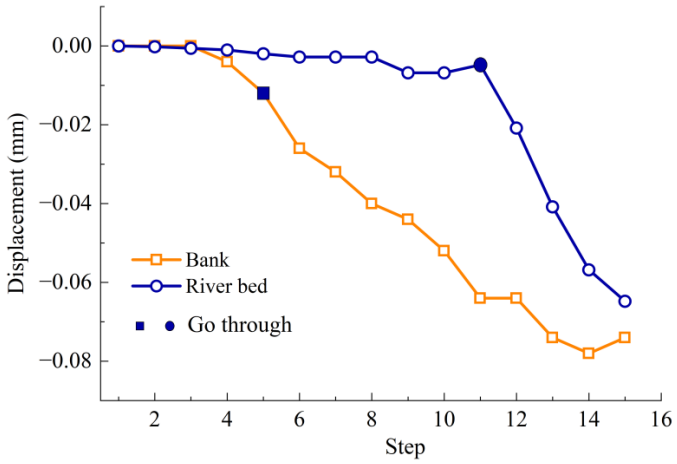

Figure 8. Shield impact on the soil surface.

4. Finite Element Analysis (FEA)

The finite element software ABAQUS 2020 was used to verify the test results. Figure 9a shows the detailed structure of the tunneling part of the model. In order to simulate the layers in numerical simulations, a 3D deformable solid element was used to represent segment and grout layers, while the shell element was used for the shield shell.

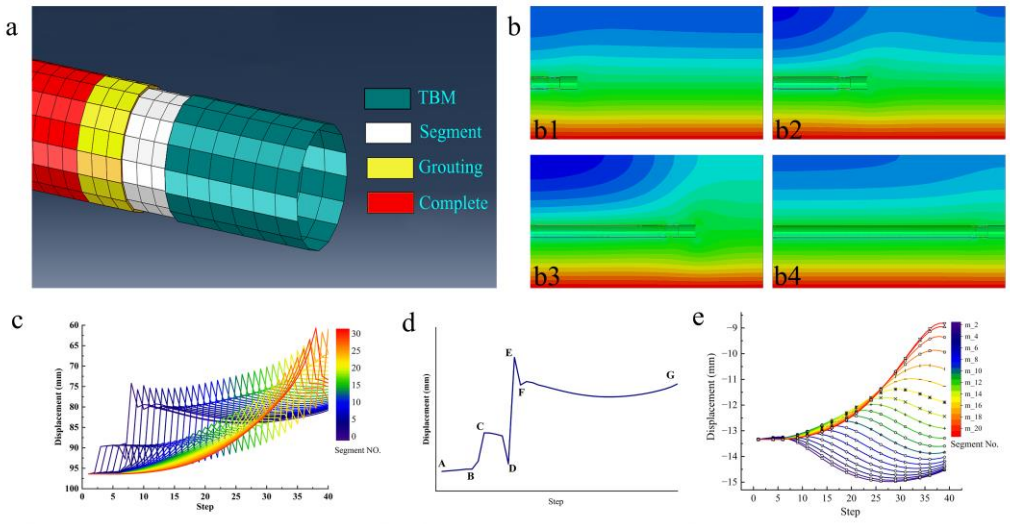

Figure 9. Finite element analysis; (**a**): finite element model; (**b**): displacement clouds during shield tunneling: (**b1**): 50 m digging distance, (**b2**): 100 m digging distance, (**b3**): 150 m digging distance, and (**b4**): 200 m digging distance; (**c**): impact of shield tunneling on surrounding soil; (**d**): Deformation pattern of surrounding soil; and (**e**): impact of shield tunneling on ground settlement.

The "birth and death" method was applied to simulate tunnel construction, and the heating method was used to simulate the grouting process of the grout layer. The FEA model is 50 m wide, 70 m deep, and 120 m long, and the inner diameter of the tunnel tube piece is 5.5 m, the outer diameter of the tunnel tube piece is 6 m, and the outer diameter of the shield machine is 6.28 m. As shown in Figure 9a, the shield model, tail segment, and grout layer are activated during the simulated excavation. The shield tail gap is simulated by the gap between the tunnel and the surrounding ground. A thermal load is applied to the grout layer, which expands under temperature and grouting pressure applied to the tunnel segment and surrounding soil. The grouting pressure is related to the modulus of elasticity of the grout, temperature, and coefficient of thermal expansion. The parameters were adjusted to achieve the required grouting pressure. The Mohr–Coulomb (MC) model was used for the soil constitutive relations, in which the MC model is the most prevalent constitutive relation in tunnel simulation [20–22], especially for soil consisting of coarse sand, medium-coarse sand, and silty clay. So, the use of the MC model is reasonable [23].

The FEA shows that the soil in front of the shield bulges when the shield enters the soil, and the bulge in the soil becomes more and more evident with the increase in the shield distance, so there are cumulative effects. The ground behind the shield machine settles. With the increased shield distance, the settlement gradually stabilizes. The ground settlement occurs due to the shield tail gap, ground disturbance, grout hardening, etc. [24].

The displacement curves of the shield tunnel at different locations show similar trends (Figure 9d), which can be divided into five stages: unexcavated (A−B); excavated (B−C), before grouting (C−D), grouted (D−E), and completed (E−G). During the excavation phase (B−C), the unloading reaction of the soil caused the tunnel to float upward. As the shield machine left the tunnel, the shield tail gap caused the tunnel to sink (C−D). This phase is the main reason for ground subsidence. Subsequently, grouting was used to re-support the tunnel and deformed soil, slowing down soil settlement. After the completion

of grouting, the tunnel continued to settle a little (E−F), which was caused by subsequent shield tunneling.

Moreover, the shield generated an upward displacement of the soil surface ahead, with the uplift increasing as the excavation depth deepened (Figure 9e). Once the shield machine had passed through, the uplifted surface gradually dropped, resulting in a final settlement that exceeded the initial uplift. The tunnel displacement measured in the test is consistent with the FEA. Although the surface uplift before the shield passage was not measured in the test, the surface settlement after the shield passage matches the FEA results.

5. Field Test

To enhance the credibility of the test, on-site measurements were conducted at the Xi'an Metro Phase 3 project. The construction project utilized an SPB (Slurry Pressure Balance Shield) to excavate and advance from the south bank of the Weihe River toward the north bank. The site has relatively open surroundings, with a double-pier supported road bridge located above one side of the tunnel (Figure 10c). The total length of the tunnel is about 600 m. There were two lines: the left line and the right line. Monitoring was started from the southwest Weihe River along the direction of the shield tunnel. The total length of monitoring was 400 m: 140 m was river diffuse, 160 m was deep water, and 100 m was shallow water (Figure 10a). Monitoring points were placed along the tunnel axis (Figure 10d), with six points positioned above the right tunnel and six points above the left tunnel, where the right line was the first tunnel (Figure 10b).

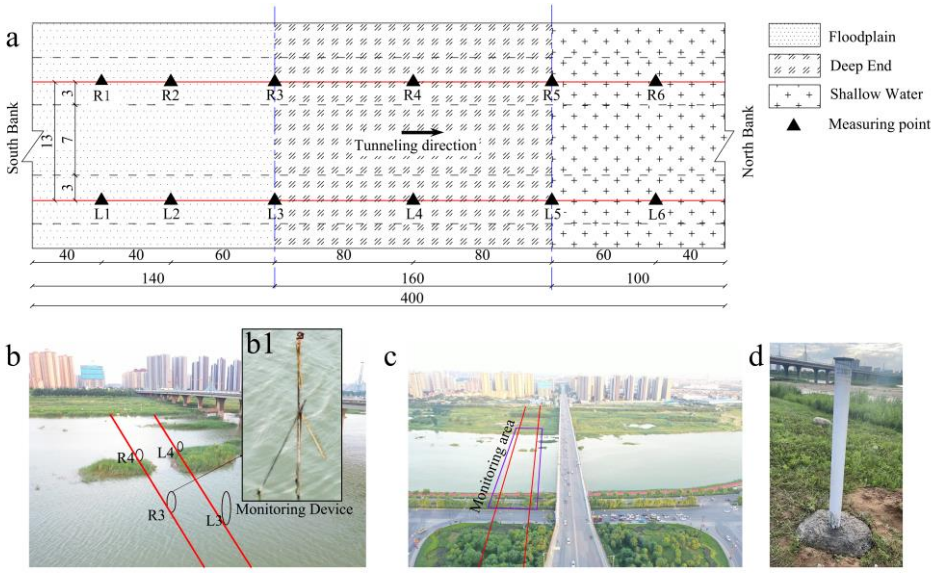

Figure 10. (**a**) Location map of measurement points; (**b**) actual measurement point photo1; (**b1**) measuring points located in the river; (**c**) monitoring range; and (**d**) monitoring points located on the riverbank.

The field test obtained the settlement data, river water level data, and tunneling speed data for six groups of measurement points (Figure 11). The results indicated that all measurement points, except for the third group (L3 and R3) (Figure 11d), showed uplift after shield passage. This observation matches the test findings. Furthermore, as the shield tunnel traversed the riverbank and deep water, a noticeable settlement occurred at all measurement points, with the settlement being more pronounced in the right line than the left line. This can be attributed to the sudden change in the soil's mechanical properties at the riverbank junction, increasing the disturbance caused by the shield. When the tunnel crossed from deep to shallow water areas, the surface settlement did not change significantly due to continuous geology change.

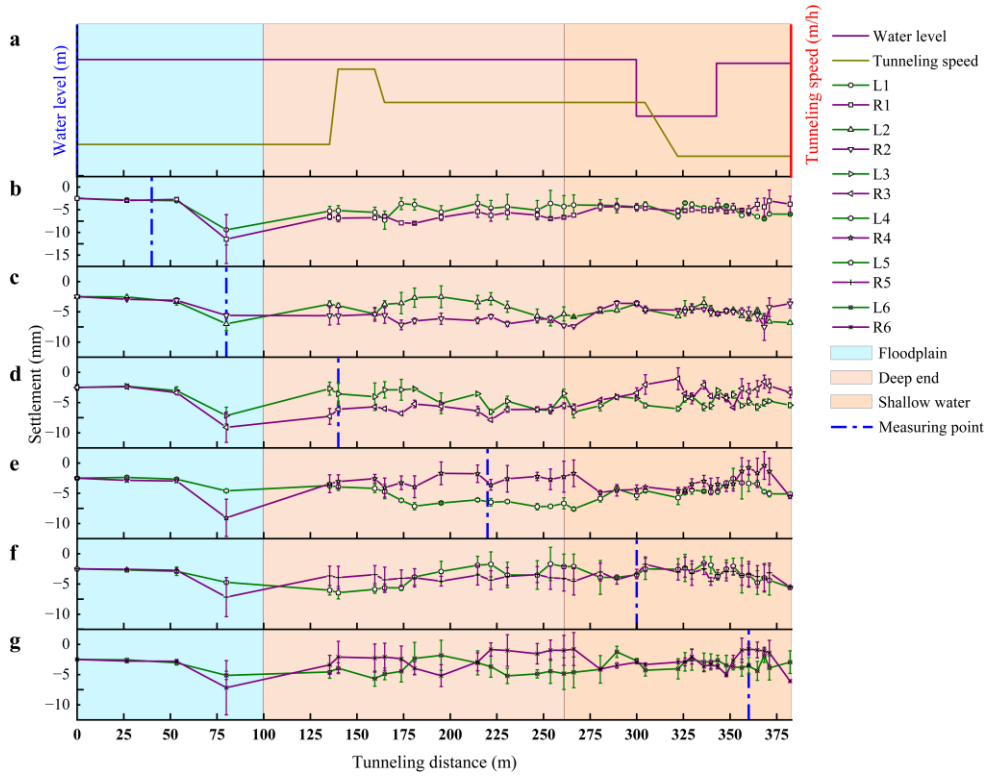

Figure 11. Field measured data: (**a**): water level map and digging speed; (**b**): measurement point 1; (**c**): measurement point 2; (**d**): measurement point 3; (**e**): measurement point 4; (**f**): measurement point 5; and (**g**): measurement point 6.

By analyzing the relationship between the left and right lines, it is observed that during the shield tunnel crossing of floodplains and shallow water, there is a minimal disparity in the settlement of measurement points on both sides. When the shield tunnel crosses the deep water, a significant difference in settlement is shown between the measurement points on the left and right lines. The analysis indicates that a shield tunnel traversing deep water causes more significant settlement and wider influence on the surrounding area.

In addition, it should be noted that the rise in water level due to precipitation and settlement difference between the left and right lines occurs simultaneously. Considering the possibility of rising water levels affecting the settlement is essential.

It is worth noting that the measured data were irregular and subjected to significant disturbances. This is because the settlement markers were disturbed by weather and rivers, thus resulting in difficulty in measuring the precision of the settlement changes. The field test cannot measure the displacement of the tunnel and soil body located underground.

6. Discussion

In order to validate the accuracy of numerical results, the FEA and field tests are compared, as shown in Figure 12. Although there are differences between the FEA and measured data, the overall trend is similar. Consequently, the FEA is considered reliable. In particular, in the river floodplain area under the influence of tunneling, the ground displacement exhibits a pattern of settlement followed by a slight uplift. The measured data show greater settlement and uplift amplitudes than the FEA. When the shield was excavated at 80 m, the field test data showed that a large settlement occurred at all measurement points, which is also verified in Figure 11, while the pattern is not found in the FEA. The reason may be the change in the underground hydrological conditions caused by the shield entering the river from the riverbank. It may also be caused by the rainy weather encountered during the project.

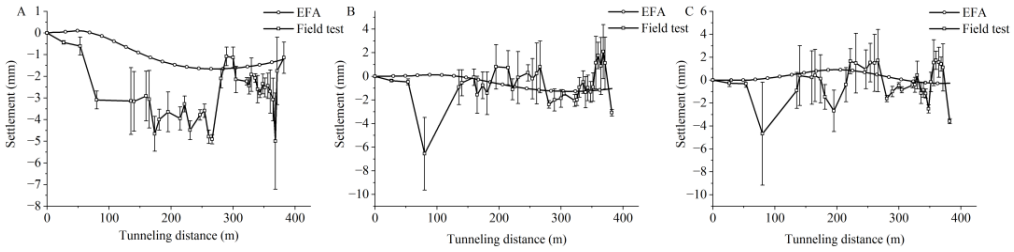

Figure 12. Comparison between finite element results and measured results (**A**). Surface deformation in the river floodplain; (**B**) surface deformation in the river channel; and (**C**) surface deformation in the shallow water area.

The deformation trends in the riverbed and shallow water areas are similar, showing a pattern of initial uplift followed by settling. It is worth noting that the uplift in the riverbed area occurred earlier, as the shield machine passed through this region before entering the shallow water area. However, the accuracy of the measured ground settlement data is affected by weather, traffic, and human activities, leading to lower precision and greater fluctuations. These fluctuations may obscure the true ground changes. Additionally, the small amount of ground settlement caused by the shield machine can easily be masked by external factors such as river erosion and vehicular traffic-induced ground deformations. Therefore, it is necessary to consider using deeper and more robust measurement points to improve the accuracy and reliability of data.

Table 4 shows the maximum surface settlements at three locations—river floodplain, river channel, and shallow water area—obtained using the three methods. It is worth noting that the ground settlements from the FEA are the lowest, while the settlements measured in the field are the largest. The maximum settlements in field tests for both the river channel and shallow water area occurred at 80 m, precisely at the transition point between the river floodplain and river channel. In the tests and FEA, the maximum settlement occurred in the last part of the shield tunnel. Additionally, Table 4 includes the final settlement values of the field test that are less than the maximum value. Despite differences in maximum ground settlements obtained using the three methods, a consistent trend emerges: ground settlement induced by the shield tunneling on the river floodplain is greater than that in the river channel. It is worth noting that a significant ground settlement occurs when the shield transitions from the river floodplain to the river channel, but this phenomenon is not detected in the tests or FEA. This settlement will be explored in future studies.

Table 4. Table of maximum ground settlement.

Settlement	Test	FEA	Field_Max	Field_End
River floodplain	3.12 mm	1.66 mm	4.99 mm	4.99 mm
River channel	2.592 mm	1.27 mm	6.55 mm	3.08 mm
Shallow water area	\	0.91 mm	5.83 mm	3.58 mm

Soil deformation during shield construction is caused by soil movement toward the excavation face, soil movement in the radial direction, the shield tail gap, deformation of the tunnel lining, and the consolidation that occurs in the case of clay soils. Due to the small diameter of the tunnel model used in this test (only 160 mm), it was challenging to apply the circumferential grout pressure. Therefore, grouting was not considered in this test, resulting in the radial movement of soil and the shield tail gap not being well-simulated in this test. The treatment in this research was using the deformation of the tunnel model with smaller stiffness to simulate the shield tail gap and the gap between the tunnel and soil. This may cause some errors, such as lateral deformation of the tunnel model and the inability to consider the effects of grouting pressure and grout hardening.

This test does not fall under the category of a rigid similarity test. Instead, it belongs to the third type of model test, which primarily focuses on a qualitative study of the displacement law concerning soil and tunnels. An accurate quantitative analysis needs a rigid similarity test. Furthermore, the tests in this paper only involved a single tunnel, while in actual subway engineering, bi-directional tunnels are common [24]. By increasing the number of pre-embedded tunnels within the test tank and adjusting the loading equipment, this test method can be extended to scaled model testing of twin-tunnel shields. It is worth noting that the test method proposed in this paper can be applied to parametric shield studies, including tunnel size, tunnel depth, and double tunnel distance [25]. Detailed research in this area will be pursued in future studies.

7. Conclusions

This paper proposed a model test method and apparatus capable of simulating the entire process of shield tunneling. Using the Xi'an Metro Phase III project in China as a case study, a model test was conducted to demonstrate its effectiveness and simulate the whole process of the shield tunnel crossing the Wei River. The displacement of the tunnel model and the ground surface were measured during the test. The test results were verified with a FEA and field measurements, and the following conclusions were obtained:

1. The scaling test model uses the combined methods of a pre-buried tunnel and discrete tunneling, which can carry out long-distance simulation of shield tunneling with a maximum simulation distance of 100 m. It can monitor and study tunnel segment settlement and ground surface deformation during the shield tunnel.
2. Soil unloading reaction causes downward deflection of the shield trajectory.
3. When the shield machine enters the river from the riverbank, the sudden change in the soil's mechanical properties leads to increased soil disturbance and causes ground surface settlement.
4. The model test results agree with the simulation and the measured results, which can provide a simple test scheme for the shield under the river and a guide for the whole process of the shield tunnel with the combination of simulation calculation and field measurement.

However, it should be acknowledged that studies of shield tunneling have multiple functions. This research only discussed the effects of shield excavation and tunnel deformation on the surrounding soil. Therefore, more work needs to be performed to improve the tests, such as grouting pressure, shield tail gap, and excavation pressure. In addition, improvements in the heating method in numerical analysis are required to simulate grouting pressure. A further study is still in progress.

Author Contributions: Conceptualization, W.L.; methodology, Y.Z.; software, W.L.; validation, Y.Z.; formal analysis, W.L.; investigation, W.L.; resources, J.M.; data curation, Y.Z.; writing—original draft preparation, W.L.; writing—review and editing, M.E.H.; visualization, W.L.; supervision, J.M.; project administration, J.M.; funding acquisition, J.M. All authors have read and agreed to the published version of this manuscript.

Funding: This research received no external funding.

Data Availability Statement: The research data for this article are included in this paper.

Conflicts of Interest: The authors declare no conflict of interest.

References

1. Feng, C.; Wang, M.; Liu, D.; Shu, D. Field Test Research of Ground Disturbance by Shield Tunnelling in Slate Strata. *Chin. J. Undergr. Space Eng.* **2018**, *14*, 138–144.
2. Hu, X.; He, C.; Peng, Z.; Yang, W.J.E. Analysis of ground settlement induced by Earth pressure balance shield tunneling in sandy soils with different water contents. *Sustain. Cities Soc.* **2019**, *45*, 296–306. [CrossRef]
3. Jin, D.; Yuan, D.; Zheng, H.; Li, X.; Ding, F. Centrifugal model tests on face stability of slurry shield tunnels under high water pressures. *Chin. J. Geotech. Eng.* **2019**, *41*, 1653–1660.

4. Han, M.S.; Kim, Y.J.; Shin, I.J.; Lee, Y.J.; Shin, Y.S.; Kim, S.H. Simulation of shield TBM tunneling in soft ground by laboratory model test. *J. Korean Tunn. Undergr. Space Assoc.* **2013**, *15*, 483–496.
5. Xiang, P.; Wei, G.; Zhang, S.; Cui, Y.; Guo, H. Model Test on the Influence of Surcharge, Unloading and Excavation of Soft Clay Soils on Shield Tunnels. *Symmetry* **2021**, *13*, 2020. [CrossRef]
6. Mair, R.J.; Taylor, R.N. Bored tunnelling in the urban environment. In Proceedings of the International Conference on Soil Mechanics & Foundation Engineering, Hamburg, Germany, 6–12 September 1997.
7. Xue, Y.; Li, X.; Qiu, D.; Ma, X.; Zhao, Y.J.G. Stability evaluation for the excavation face of shield tunnel across the Yangtze River by multi-factor analysis. *Geomech. Eng.* **2019**, *19*, 283–293.
8. Küpferle, J.; Zizka, Z.; Schoesser, B.; Röttger, A.; Alber, M.; Thewes, M.; Theisen, W. Influence of the slurry-stabilized tunnel face on shield TBM tool wear regarding the soil mechanical changes—Experimental evidence of changes in the tribological system. *Tunn. Undergr. Space Technol.* **2018**, *74*, 206–216. [CrossRef]
9. Liu, C.; Li, J.; Zhang, Z.; Li, P.; Cui, J.; Liu, H.; Yang, Y. Model tests on tail-grouting process during URUP shield tunneling in soft soil. *Tunn. Undergr. Space Technol.* **2020**, *103*, 103451. [CrossRef]
10. Li, L.; Sun, S.; Wang, J.; Yang, W.; Song, S.; Fang, Z. Experimental study of the precursor information of the water inrush in shield tunnels due to the proximity of a water-filled cave. *Int. J. Rock Mech. Min. Sci.* **2020**, *130*, 104320. [CrossRef]
11. Yang, Z.-S.; Peng, F.-L.; Qiao, Y.-K.; Hu, Y.-Y. A new cryogenic sealing process for the launch and reception of a tunnel shield. *Tunn. Undergr. Space Technol.* **2019**, *85*, 406–417. [CrossRef]
12. Kim, J.J.; Ryu, H.H.; Kim, G.Y.; Hong, S.Y.; Jeong, J.H.; Bae, D.S. Development of penetration rate model and optimum operational conditions of shield TBM for electricity transmission tunnels. *J. Korean Tunn. Undergr. Space Assoc.* **2020**, *22*, 623–641.
13. Zhao, T.; Ding, W.; Qiao, Y.; Duan, C. A large-scale synchronous grouting test for a quasi-rectangular shield tunnel: Observation, analysis and interpretation. *Tunn. Undergr. Space Technol.* **2019**, *91*, 103018. [CrossRef]
14. Xu, Q.; Zhu, H.; Ding, W.; Ge, X. Laboratory model tests and field investigations of EPB shield machine tunnelling in soft ground in Shanghai. *Tunn. Undergr. Space Technol.* **2011**, *26*, 1–14. [CrossRef]
15. Ding, W.; Duan, C.; Zhu, Y.; Zhao, T.; Huang, D.; Li, P. The behavior of synchronous grouting in a quasi-rectangular shield tunnel based on a large visualized model test. *Tunn. Undergr. Space Technol.* **2019**, *83*, 409–424. [CrossRef]
16. Lü, X.; Zhou, Y.; Huang, M.; Zeng, S. Experimental study of the face stability of shield tunnel in sands under seepage condition. *Tunn. Undergr. Space Technol.* **2018**, *74*, 195–205. [CrossRef]
17. Zhang, D.M.; Chen, S.; Wang, R.C.; Zhang, D.M.; Li, B.J. Behaviour of a large-diameter shield tunnel through multi-layered strata. *Tunn. Undergr. Space Technol.* **2021**, *116*, 104062. [CrossRef]
18. Tian, Z.; Yu, C.; Zhang, B.; Zhao, Q.; Wang, Z. Analysis of Surface and Building Deformation by Shield Tunneling through Geology. *Appl. Sci.* **2023**, *13*, 11155. [CrossRef]
19. Lu, Y.; Yu, P.; Zhang, Y.; Chen, J.; Liu, T.; Wang, H.; Liu, H. Deformation analysis of underwater shield tunnelling based on HSS model parameter obtained by the Bayesian approach. *Front. Mar. Sci.* **2023**, *10*, 1195496. [CrossRef]
20. David, T.K.; Krishnamoorthy, R.R.; Jais, M. Finite Element Modelling of Soil-Structure Interaction. *J. Teknol.* **2015**, *76*, 55–63. [CrossRef]
21. Forcellini, D.; Alzabeebee, S. Seismic fragility assessment of geotechnical seismic isolation (GSI) for bridge configuration. *Bull. Earthq. Eng.* **2022**, *21*, 3969–3990. [CrossRef]
22. Goktepe, F.; Sahin, M.; Celebi, E.J.B.o.E.G.; Environment, t. Small shaking table testing and numerical analysis of free-field site response and soil-structure oscillation under seismic loading. *Bull. Eng. Geol. Environ.* **2020**, *79*, 2949–2969. [CrossRef]
23. Ti, K.S.; Huat, B.B.; Noorzaei, J.; Jaafar, M.S.; Sew, G.S. A Review of Basic Soil Constitutive Models for Geotechnical Application. *Electron. J. Geotech. Eng.* **2009**, *14*, 2969.
24. Alsirawan, R.; Sheble, A.; Alnmr, A. Two-Dimensional Numerical Analysis for TBM Tunneling-Induced Structure Settlement: A Proposed Modeling Method and Parametric Study. *Infrastructures* **2023**, *8*, 88. [CrossRef]
25. Alnmr, A.; Sheble, A.; Ray, R.; Ahmad, H. Parametric Investigation of Interaction between Soil-Surface Structure and Twin Tunnel Excavation: A Comprehensive 2D Numerical Study. *Infrastructures* **2023**, *8*, 124. [CrossRef]